Supporting Information

MXene and MoS_{3-x} coated 3D-printed hybrid electrode for solid-state asymmetric supercapacitor

*Kalyan Ghosh, Martin Pumera**

Dr. K. Ghosh, Prof. M.Pumera
Future Energy and Innovation Laboratory, Central European Institute of Technology, Brno University of Technology, Purkyňova 123, 61200 Brno, Czech Republic
E-mail: pumera.research@gmail.com

Prof. M. Pumera
3D printing & Innovation Hub, Department of Chemistry and Biochemistry, Mendel University in Brno, Zemedelska 1, 61300, Brno, Czech Republic

Prof. M. Pumera
Department of Chemical and Biomolecular Engineering, Yonsei University, 50 Yonsei-ro, Seodaemun-gu, Seoul 03722, South Korea

Prof. M. Pumera
Department of Medical Research, China Medical University Hospital, China Medical University, No. 91 Hsueh-Shih Road, Taichung 40402, Taiwan

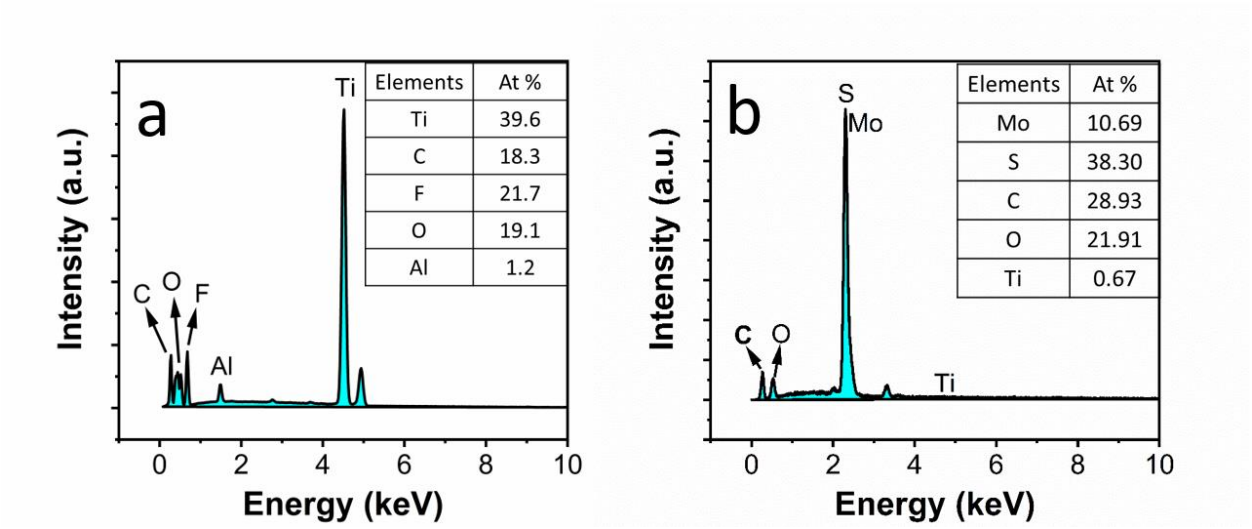

Figure S1. Energy-dispersive X-ray spectroscopy of (a) Ex-$Ti_3C_2T_x$ MXene and (b) MoS_{3-x} coated 3D-printed nanocarbon framework (MoS_{3-x}@3DnCF), inset table shows the atomic percentages of the constituent elements.

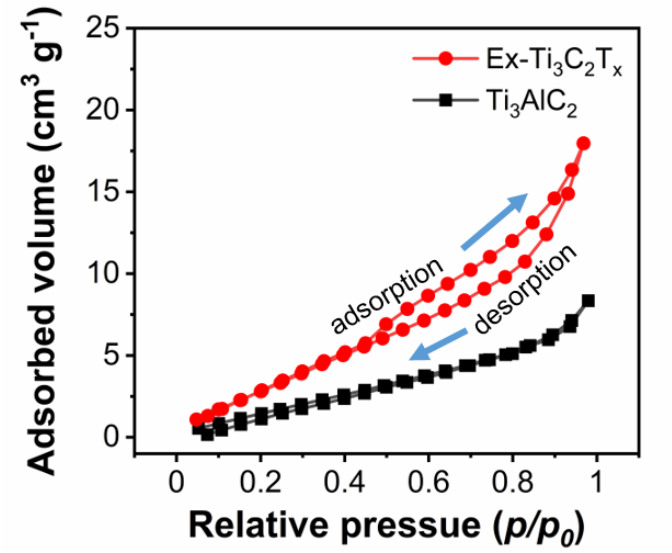

Figure S2. Brunauer-Emmett-Teller (BET) nitrogen adsorption-desorption isotherm of Ti_3AlC_2 and Ex-$Ti_3C_2T_x$.

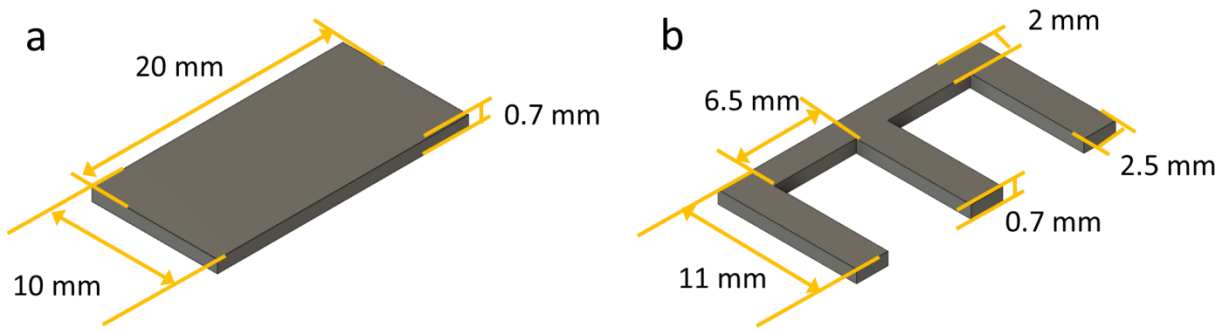

Figure S3. Dimensions of the 3D-printed electrodes (a) rectangular shape and (b) interdigitated shape.

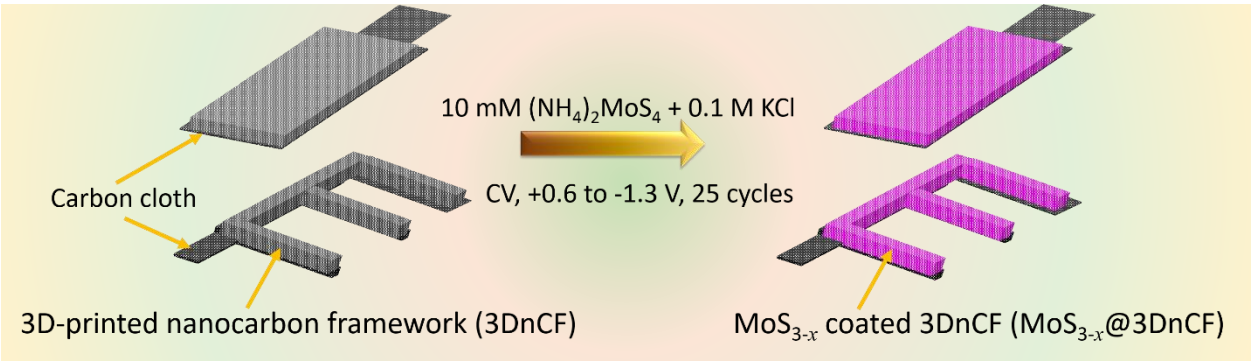

Figure S4. Schematic diagram for electrodeposition of MoS_{3-x} on 3D-printed nanocarbon framework.

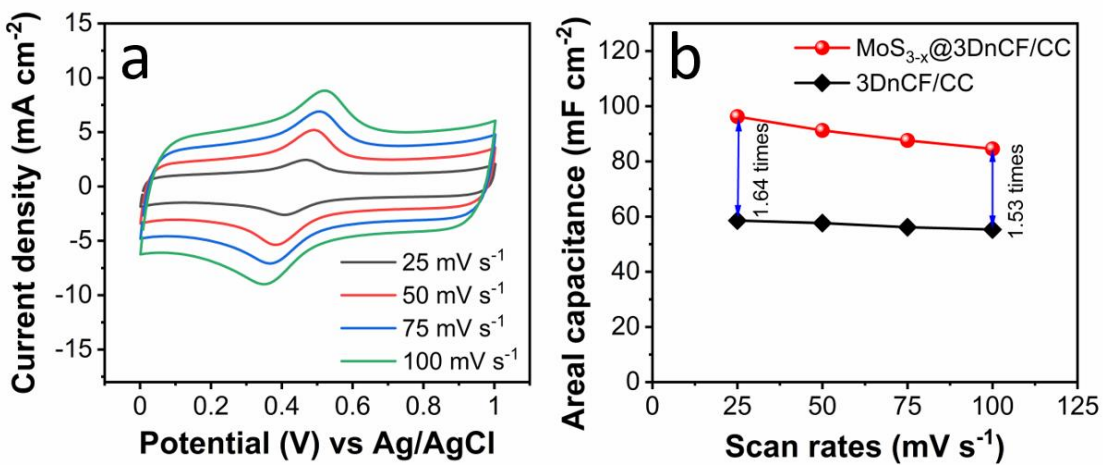

Figure S5. (a) Cyclic voltammetry of 3D-printed nanocarbon framework electrode (3DnCF/CC) in 1 M H_2SO_4 and (b) comparison of areal capacitance of blank 3DnCF/CC and MoS_{3-x}@3DnCF/CC at different scan rates.

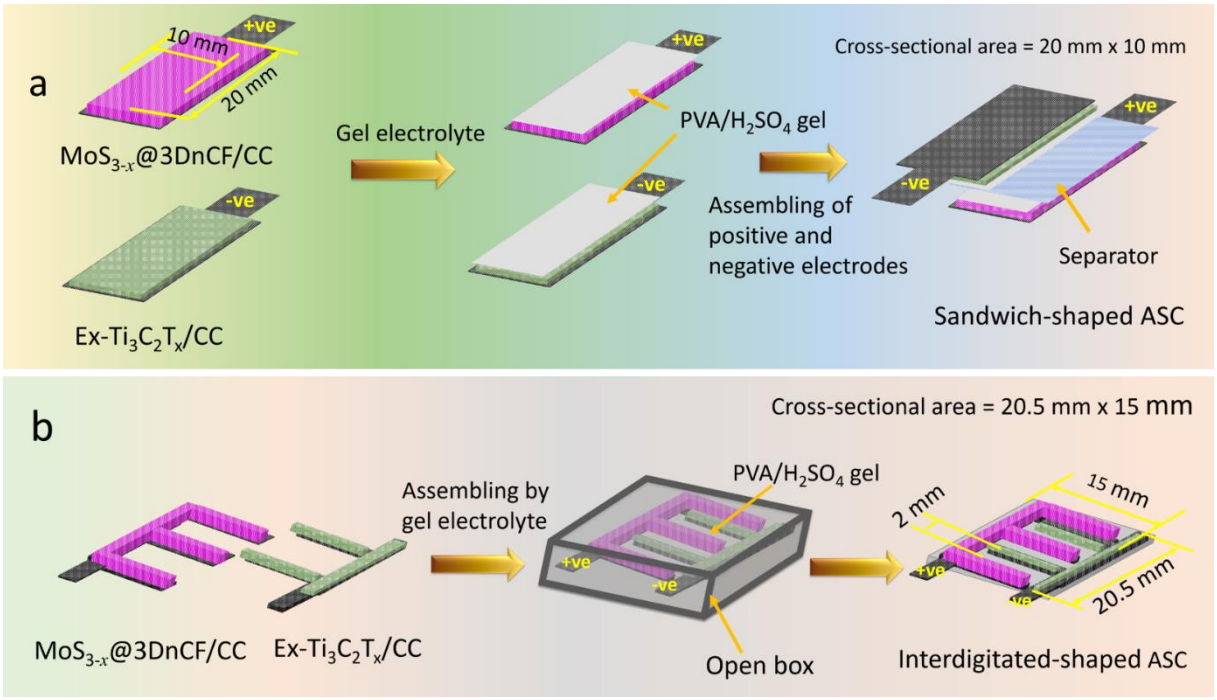

Figure S6. Schematic diagram of fabrication of solid-state asymmetric supercapacitor (a) sandwich- (b) interdigitated-configurations.

The $Ti_3C_2T_x$/CC and MoS_{3-x}@3DnCF/CC electrodes show >10^3 times of capacitance compared to blank CC.

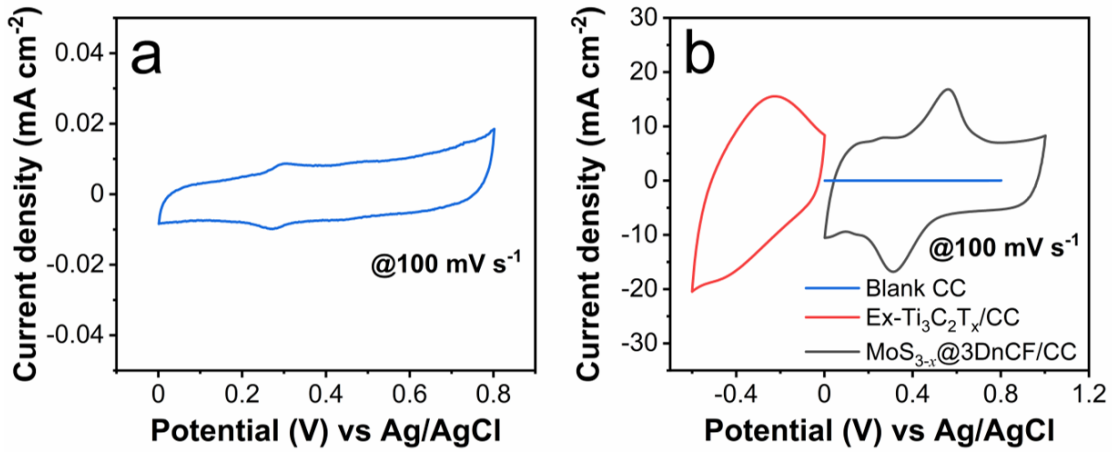

Figure S7. (a) Cyclic voltammetry of blank carbon cloth (CC) in 1 M H_2SO_4 and (b) comparison of cyclic voltammetry of blank CC, Ex-$Ti_3C_2T_x$/CC and MoS_{3-x}@3DnCF/CC at scan rate of 100 mV s^{-1}.

Ti_3AlC_2 to $Ti_3C_2T_x$ synthesis mechanism:

$$Ti_3AlC_2 + HF \rightarrow Ti_3C_2 + AlF_3 + 3/2\ H_2 \quad \text{(S1)}$$

$$Ti_3C_2 + 2\ H_2O \rightarrow Ti_3C_2(OH)_2 + H_2 \quad \text{(S2)}$$

$$Ti_3C_2 + 2HF \rightarrow Ti_3C_2F_2 + H_2 \quad \text{(S3)}$$

In three-electrode test set up, the areal capacitance, $C_{electrode}^{areal}$ [F cm^{-2}] of positive or negative electrode was calculated from the cyclic voltammetry (CV) study using Equation-S4:[1-3]

$$C_{electrode}^{areal} = \frac{\int_{V_1}^{V_2} I(V)dV}{v\,(V_2 - V_1)A} \quad \text{(S4)}$$

where, $I(V)$ is the current [mA] in the cathodic sweep of the cyclic voltammogram for positive electrode and $I(V)$ is the current [mA] in the anodic sweep of the cyclic voltammogram for negative electrode, v is the scan rate [mV s^{-1}], A is the active geometrical area [cm^2] of the electrode, and V_1 and V_2 are the potential [V] limits in the CV study. The A in the denominator of Equation-S4 is replaced with active mass m [g] of the electrode material to calculate the gravimetric capacitance, $C_{electrode}^{gravimetric}$ [F g^{-1}].

Moreover, the $C_{electrode}^{areal}$ [F cm^{-2}] of the positive or negative electrode was calculated from the constant current discharging curve of galvanostatic charge-discharge (GCD) study using Equation-S5:[2]

$$C_{electrode}^{areal} = \frac{I\,\Delta t}{\Delta V\,A} \quad \text{(S5)}$$

where, I is the constant discharge current [A], Δt is the total discharging time [s], ΔV is the discharge voltage [V] range and A is the active geometrical area [cm^2] of the electrode. The 'A' in the denominator of Equation-S5 was replaced by active mass 'm' [g] of the electrode material to calculate the $C_{electrode}^{gravimetric}$ [F g^{-1}].

In two-electrode test set up, the areal cell capacitance, C_{cell}^{areal} [F cm^{-2}] was calculated from the constant current discharging curve of GCD experiment using the Equation-S6:[3, 4]

$$C_{cell}^{areal} = \frac{I\,\Delta t}{\Delta V\,A} \quad \text{(S6)}$$

where, I is the constant discharge current [A], Δt is the total discharging time [s], ΔV is the range of discharge voltage [V] and A [cm^2] is the active geometrical area of the cell. The volumetric capacitance, $C_{cell}^{volumetric}$ [F cm^{-3}] and the gravimetric capacitance, $C_{cell}^{gravimetric}$ [F g^{-1}] were calculated replacing A in the denominator of Equation-S6 with total volume of the cell which includes electrodes, current collectors, separator and electrolyte, V_{cell} [cm^3], and total active mass, m [g] of the two electrodes, respectively.

The areal energy density, E_{cell}^{areal} [mWh cm^{-2}] was calculated from the cell capacitance using the Equation-S7.[3,5, 6]

$$E_{cell}^{areal} = 0.5 \times C_{cell}^{areal} \times \Delta V^2 \times \frac{1000}{3600} \quad \text{(S7)}$$

The volumetric energy density, $E_{cell}^{volumetric}$ [mWh cm^{-3}] and gravimetric energy density, $E_{cell}^{gravimetric}$ [Wh kg^{-1}] were calculated replacing C_{cell}^{areal} in Equation-S7 with $C_{cell}^{volumetric}$ [F cm^{-3}] and $C_{cell}^{gravimetric}$ [F g^{-1}], respectively.

The areal power density [mW cm^{-2}] wad calculated using Equation-S8.[3,5]

$$P_{cell}^{areal} = \frac{E_{cell}^{areal}}{t} \times 3600 \quad \text{(S8)}$$

where, t is the discharge time [s].

The volumetric power density, $P_{cell}^{volumetric}$ [mW cm^{-3}] and gravimetric power density, $P_{cell}^{gravimetric}$ [W kg^{-1}] were calculated replacing E_{cell}^{areal} in Equation-S8 with $E_{cell}^{volumetric}$ [mWh cm^{-3}] and $E_{cell}^{gravimetric}$ [Wh kg^{-1}].

The real part, $C'(\omega)$ and imaginary part, $C''(\omega)$ of capacitances were calculated from Equation S9 and S10, respectively.[7]

$$C'(\omega) = \frac{-Z''(\omega)}{\omega |Z(\omega)|^2} \quad \text{(S9)}$$

$$C''(\omega) = \frac{Z\prime\,(\omega)}{\omega|Z(\omega)|^2} \quad \text{(S10)}$$

where, $Z(\omega)$ is the impedance, $Z'(\omega)$ and $Z''(\omega)$ are the real part and imaginary part of $Z(\omega)$, respectively. ω is the angular frequency; where, $\omega = 2\pi f$ and f is the frequency [Hz].

Table S1. High resolution core-level X-ray photoelectron spectroscopy peak fitting results of Ex-$Ti_3C_2T_x$: peak positions, peak fitting full widths at half maximum (FWHM), assigned species and their quantified composition. Bold font shows the contribution from $Ti_3C_2T_x$.

Region	Binding energy (eV)	FWHM (eV)	Peak assignment	At %
Ti $2p_{3/2}$ ($2p_{1/2}$)	**455.5 (461.5)**	**1.09 (1.48)**	**Core Ti as well as Ti linked to terminal groups (OH, F, O)) (Ti−C)**	**10.871**
	456.3 (462.0)	**1.56 (1.80)**	**Ti (II)**	**17.024**
	457.6 (463.3)	**2.02 (1.82)**	**Ti (III)**	**14.765**
	459.3 (465.0)	1.50 (1.95)	($TiO_{2-x}F_{2x}$)	6.742
	460.5 (466.2)	0.93 (1.3)	TiF_{3+x} (TiF_3)	2.105
O 1s	**530.1**	**0.84**	**Oxygen on bridge site (C−Ti−O_x)**	**4.403**
	530.9	**1.71**	**$TiO_{2-x}F_{2x}$**	**4.535**
	532.0	**1.44**	**Hydroxyl group (C−Ti−OH)**	**2.133**
	533.1	1.47	Adventitious oxygen (C−O)	1.603
	534.4	1.22	Adsorbed H_2O (Ads. H_2O)	0.344
C 1s	**282.3**	**0.60**	**C from MXene (C−Ti−F_x)**	**9.427**
	282.8	**1.63**	**C from MXene (C−Ti−O_x)**	**4.712**
	284.3	0.84	C−C (sp^2)	3.08
	285.0	1.06	Amorphous C C−C (sp^3)	6.547
	285.8	2.17	Adventitious C (C−O)	4.769
F 1s	**685.4**	**1.16**	**F from MXene (C−Ti−F_x)**	**4.356**
	686.0	2.39	($TiO_{2-x}F_{2x}$)	1.679
	686.7	2.15	Unidentified fluorinated phase[8] (M−F_x)	0.899

Table S2: Volumetric and gravimetric capacitance, energy density and power density of sandwich-configuration asymmetric cell.

Volumetric				Gravimetric			
Current density ($mA\ cm^{-3}$)	Capacitance ($mF\ cm^{-3}$)	Energy density ($\mu Wh\ cm^{-3}$)	Power density ($mW\ cm^{-3}$)	Specific current ($mA\ g^{-1}$)	Capacitance ($mF\ g^{-1}$)	Energy density ($Wh\ kg^{-1}$)	Power density ($W\ kg^{-1}$)
1.66	1067.70	379.63	1.33	14.23	9120.51	3.24	11.39
3.33	758.33	269.63	2.66	28.47	6477.79	2.30	22.78
10.00	600.00	213.33	8.00	85.42	5125.28	1.82	68.34
16.66	541.66	192.59	13.33	142.37	4626.99	1.64	113.89
23.33	437.50	155.55	18.66	199.31	3737.19	1.33	159.45
33.33	458.33	162.96	26.66	284.74	3915.15	1.39	227.79
50.00	437.50	155.55	40.00	427.11	3737.19	1.33	341.68

References

[1] V. Khomenko, E. Frackowiak, F. Beguin, *Electrochim. Acta*. **2005**, *50*, 2499.

[2] S. Zhang, N. Pan, *Adv. Energy Mater.* **2015**, *5*, 1401401.

[3] A. Laheäär, P. Przygocki, Q. Abbas, F. Béguin, *Electrochem. Commun.* **2015**, *60*, 21.

[4] K. Ghosh, C. Y. Yue, M. M. Sk, R. K. Jena, S. Bi, *Sustain. Energy Fuels* **2018**, *2*, 280.

[5] K. Ghosh, C. Y. Yue, *Electrochim. Acta*. **2018**, *276*, 47.

[6] K. Ghosh, C. Yue, M. Sk, R. Jena, *ACS Appl. Mater. Interfaces* **2017**, *9*, 15350.

[7] P. Taberna, P. Simon, J.-F. Fauvarque, *J. Electrochem. Soc.* **2003**, *150*, A292.

[8] M. Benchakar, L. Loupias, C. Garnero, T. Bilyk, C. Morais, C. Canaff, N. Guignard, S. Morisset, H. Pazniak, S. Hurand, *Appl. Surf. Sci.* **2020**, *530*, 147209.